Zhongguo Kuangye Daxue Xuebao
Journal of China University of Mining and Technology

2024 | Vol 29 | Issue 4 | Page 121-135
Journal Homepage: https://zkdx.ch/
DOI: 10.1654/zkdx.2024.29.4-11

Synthesis, Spectroscopic Characterization, and Biological Applications of Some Metal Complexes: Biochemical and Molecular Docking Studies

Mohammed H. H. Abu-Setta*
Department of Chemistry, Faculty of Science, Menoufia University, Shebin El -Kom, Egypt
*Corresponding author

Abdou S. El Tabl
Department of Chemistry, Faculty of Science, Menoufia University, Shebin El -Kom, Egypt

Esraa O. Ahmed
Department of Chemistry, Faculty of Science, Menoufia University, Shebin El -Kom, Egypt

Eman A. Mohamed
Basic science department- International academy for engineering and media science

Ahmed G. Abd El-Nasser
Department of Chemistry, Faculty of Science, Menoufia University, Shebin El -Kom, Egypt

Ahmed M. Ashour
Department of Chemistry, Faculty of Science, Menoufia University, Shebin El -Kom, Egypt

Abstract
The solid complexes formed from N, N'-(1,2-phenylene) bis-(3,4,5-trihydroxybenzamide) bio active ligand (HL) expected to be potent anti-inflammatory and Mn(II), Fe(III), Ni(II), Cu(II) and Zn(II) have been synthesized and characterized by elemental and thermal analysis along with different spectroscopic techniques. The cytotoxic activity of some solid complexes against experimental animals (Albino rats) prostate cell cancer was extensively studied and expressed as lethal dose 50 (LD_{50}). The acute intra-peritoneal toxicity of the chosen complexes was done using 21 experimental rat animals. After administration of the chosen complexes' concentrations, the rats were observed for toxic effects after 24h of treatment. Molecular docking studies against prostate cancer cell line (PC-3) had been done and compared to the practical data obtained.

Keywords
Hydroxy amide ligand, Phenolic acids, Complexes, Cytotoxicity, Biological activity, Prostate cancer, molecular docking

1. Introduction
Gallic acid is a secondary naturally occurring metabolite that is widely extracted from a variety of nuts, fruits and plants. It belongs to the phenolic chemical class, and has drawn more and more attention lately due to its potent anti-inflammatory [1-3]. Now a day, in addition to long-term consequences, treatment failure and rising resistance to antibiotics and anticancer medications which lead to higher financial and medical expenses, hospitalization, necessitating the development of novel strategies. The World Health Organization (WHO) estimates that, due to the significance of antibiotic resistance, fatalities from resistant bacterial infections would overtake all other causes of death worldwide by 2050 if this issue is not resolved [4]. A common explanation for the rise in pathogenic microorganism resistance is the improper use of antibiotics and the spread of resistance inside and between people. Considering that the industry's efforts to produce novel antibiotics are both expensive and have failed to draw in investors, to stop the development and spread of drug resistance, stop bacterial growth, and extend the effectiveness of traditional antibiotics, new approaches are required [5, 6], One of the most significant natural polyphenols is Gallic acid. Following the Swedish chemist Carl Wilhelm Scheele's 1786 discovery of GA in plants, research on [7] discuss the role of GA and its derivatives. Arrangement of hydroxyl groups in the ring affect the stability of radicals which are formed by the loss of Hydrogen to

the free radicals Electrometric effects mean that the hydroxyl groups which found in ortho position confers high stability Electrometric effects mean that the ortho position of hydroxyl groups confers high stability to the radicals. Regarding hydroxyl groups, the higher the number, the stronger antioxidant, and other properties [8, 9]. The antibacterial activity, plant polyphenols can act against bacterial cells through several mechanisms, such as interaction with bacterial cell walls and proteins, alteration of the cytoplasmic functions and permeability of membrane, inhibition energy of metabolism and damage of DNA or inhibition synthesis of nucleic acids by bacteria cells. At the DNA level, the planarity of the molecule and the hydrophobic core mean that polyphenols can penetrate the DNA helix during the replication, recombination, repair, and transcription mechanisms. Moreover, hydroxyl groups of phenolic compounds [10]. Antibacterial activity of polyphenols depends on their chemical structure [11]. An augmented activity can be obtained by the addition of new functional groups, hydrolysis or metal chelation, leading to enhanced interactions with different bacterial cell targets [12]. The aim of the present research is to prepare and spectroscopically characterize new metal complexes of hydroxy amide ligand and to investigate their cytotoxic effects against prostate cell cancer in experimental animals.

2. Experimental

All chemicals employed for the preparation of the ligand and its complexes were of higher synthetic grade (Merck, Alderich or sigma) and were used without further purification. The ligand, N, N'-(1,2-phenylene) bis-(3,4,5-trihydroxybenzamide) (HL) was prepared as by ……. as shown in the following scheme:

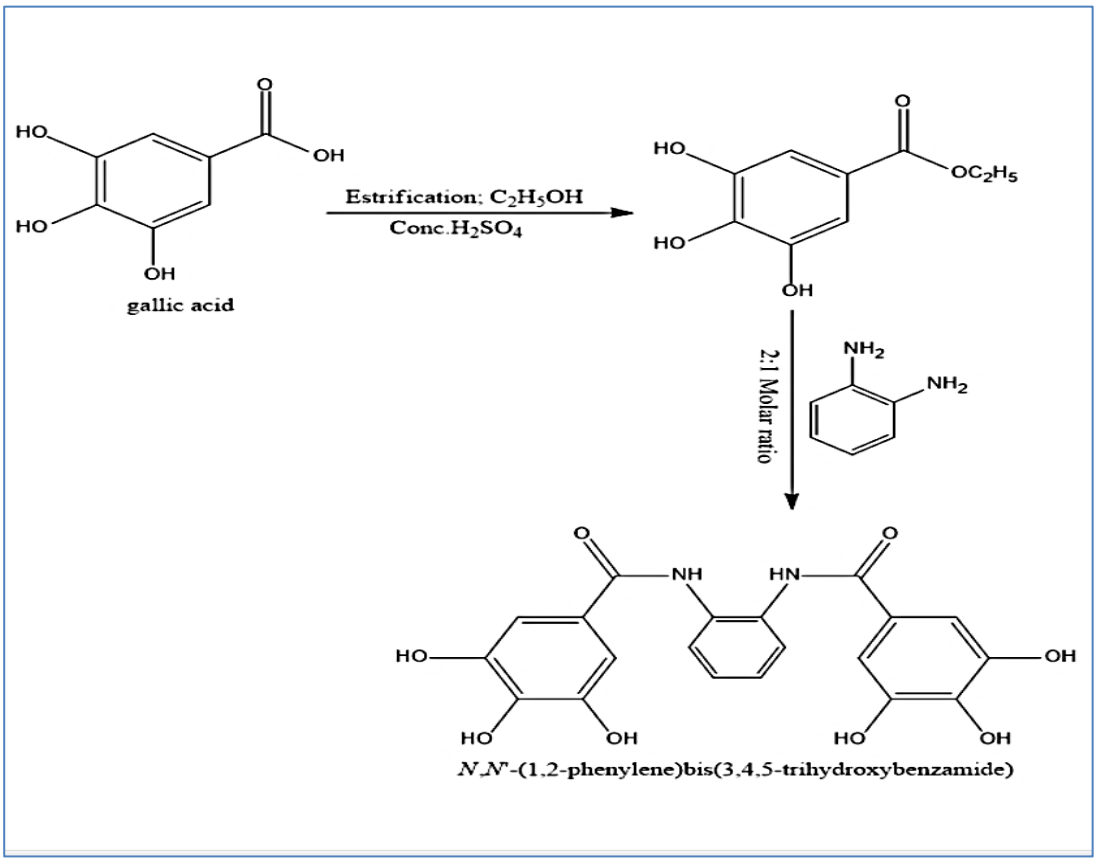

Mn(II), Fe(III), Ni(II), Cu(II) and Zn(II) have been synthesized by refluxing equimolar quantities of the ligand (HL) with $MnSO_4.2H_2O$, $FeCl_3.2H_2O$, $Ni(CH_3COO)_2.4H_2O$, $CuCl_2.2H_2O$ and $ZnSO_4.2H_2O$ in hot ethanolic solution of the following. The refluxing times varied from 2 to 4 h depending on the nature of metal ion. 3 mL of O-phenylene diamine were added to the reaction mixture to initiate precipitation of complex. The precipitates, were filtered off, washed with ethanol then by diethyl ether and dried in vacuum desiccators over P_4O_{10}.

Elemental analyses (C, H, N and Cl) were determined at The Regional Center for Mycology and Biotechnology (RCMB), Al - Azhar University, Cairo, Egypt. The IR spectra were measured as KBr pellets using a Bruker spectrophotometer (4000-400 cm^{-1}) at central laboratory, Faculty of Science-Menoufia University. ^{1}H-NMR spectra of the ligand and its Zn(II) complexe were obtained with Bruker R32-90-MHz spectrophotometer at Microanalytical Unit - FOPCU- NMR laboratory. Mass spectra were recorded using Agilent mass spectrometer provided with data system at central laboratory Faculty of Science-Menoufia University. Thermal analyses (DTA and TGA) were carried out using air as an atmosphere using Shimadzu DT-30 thermal analyzer from 30 to 800°C with heating rate of 10°C per minute at central laboratory, Faculty of Science-Menoufia University. Magnetic susceptibilities were measured at 25°C by the Gouy method using mercuric tetrathiocyanatocobalt (II) as the magnetic susceptibility standard. Diamagnetic corrections were estimated from Pascal's constant [13]. The ESR spectra of solid complexes at room temperature were recorded using a Varian E-109 spectrophotometer; DPPH was used as a standard material.

3. Biological Activity

3.1 Toxicity study

Toxicity studies of copper (II) complex (2), zinc (II) complex (13) and Iron (II) complex (11) were performed by dissolving the complexes in DMSO and then diluted by sterile saline 0.9 % NaCl in a maximum concentration of 0.2% by volume to be able to be injected intra peritoneal.

3.2 Animals

Forty-nine healthy male albino rats 8 weeks old (180 ± 5 g) were purchased from National Cancer Institute, Cairo, Egypt. Rats were housed in cages at regulated temperature (22- 25 °C). They were kept under good ventilation under a photoperiod of 12hr light/12hr darkness schedule with lights-on from 06:00 to 18:00. They all received a standard laboratory diet (60% ground corn meal, 10% bran, 15% ground beans, 10% corn oil, 3% casein, 1% mineral mixture and 1% vitamins mixture), purchased from Meladco Feed Company (Obour City, Cairo, Egypt) and supplied with water ad libitum throughout the experimental period.

3.3 Acute Toxicity Study

The lethal dose 50, (LD_{50}) of the studied compounds was determined as described by Akhila et al [46]. The acute intra-peritoneal toxicity of the chosen complexes was done on 21 animals (7 per group). The chosen complexes were administrated with graded doses ranged from 1×10^{-6} to 1×10^{-4} mmole/L/Kg body weight under the same environmental conditions. More doses were not possible due to poor solubility in case of higher concentrations. After administration of the chosen complexes' concentrations, the rats were observed for toxic effects after 24h of treatment. The toxicological effects were observed in terms of mortality and expressed as lethal dose 50 (LD50).

3.4 Experimental Design

28 animals were allowed 10 days for adaptation. They were then randomly distributed into 4 equal groups, 7 rats each. The animal groups were recognized as follows:

Group 1 (Control): Normal healthy animals injected intra peritoneal with 0.2% solution of DMSO dissolved in sterile 0.9% NaCl saline for 6 weeks.

Group 2: Each animal was injected intra peritoneal with 1x10-5mmole/L of Cu (II) complex (2) for 6 weeks.

Group 3: Each animal was injected intra peritoneal with 1x10-5mmole/L of Zn (II) complex (13) for 6 weeks.

Group 4: Each animal was injected intra peritoneal with 1x10-5mmole/L of Fe (II) complex (11) for 6 weeks.

3.5 Blood Collection

At the end of the experimental period, animals were fasted overnight prior to dissection under light isoflurane anesthesia. Blood was drawn from the venacava and centrifuged at 3000g for 10 min; whole EDTA blood was collected for hematological studies.

3.6 Biochemical Analyses

Liver enzymes activities, aspartate aminotransferase (AST) and alanine aminotransferase (ALT) were estimated using kinetic kits purchased by Human Diagnostic Kits, Germany [47]. The liver functions, albumin concentration and kidney functions, blood urea and serum creatinine were measured using Diamond Diagnostic kits, Egypt. All biochemical analyses were determined using a Biosystems BTS-350 Spectrophotometer.

3.7 Hematological Analyses

Hemoglobin concentration (Hb) was determined using Drabkin's solution on a Biosystems BTS-350 Spectrophotometer [49], red blood corpuscles count (RBCs), total leucocytes count (TLC) and platelets count (PLTs) were determined manually [48].

3.8 Statistical Analysis

Data were subjected to statistical significance tests using one-way analysis of variance (ANOVA), followed by Duncan's multiple range test. The statistical analysis was carried out using SPSS 20.00 software. The results were expressed as mean ± SD and the differences were considered significant at $P \leq 0.05$ [49].

3.9 Molecular Docking

The 6XXO protein (prostate cancer protein) was docked with the ligand (HL) and some of its complexes using Moldock score Protein basic local alignment search tool (BLASTp) search, multiple sequence alignment (MSA), and phylogenetics were further carried out to analyze the diversity of this marker and determine its conserved domains as suitable target regions.

4. Results and Discussion

4.1 Studies on the Metal Complexes in Solid State

4.1.1 I-Structure Elucidation

The solid complexes of Mn(II), Fe(III), Ni(II), Cu(II) and Zn(II) with the ligand (HL) under study were prepared by [1:1] stoichiometric ratios then characterized by the following techniques:

- *Elemental analysis and molar conductivity*

All the complexes are colored, stable in air and have high decomposition points (> 350oC). They are slightly soluble in dimethylsulphoxide (DMSO) and dimethylformamide (DMF) but paringly soluble in other common organic solvents. The proposed formula were firstly confirmed by both elemental analysis and molar conductivity. Elemental analysis (Table 1) show satisfactory agreement between the calculated and found values of C,H, N and M percentages.

The molar conductance (Λm); ohm-1cm2mol-1 of the studied complexes were measured in solutions of DMSO. The values shown in Table (1) indicate the non ionic nature of the complexes formed with divalent metal ions while Fe3+ complex is ionic in nature.

Table 1 Elemental analysis and molar conductivities of complexes Mn(II), Fe(III), Ni(II), Cu(II) and Zn(II)with the ligand HL

Complex	Tentative formula	M.Wt.	Elemental analysis*				Λ_m*
			%C	%H	%N	%M	
[HL],	$C_{20}H_{16}N_2O_8$	412	58.47 (58.25)	4.15 (3.91)	7.07 (6.79)	----	
[(HL)Mn $(SO_4)_2(H_2O)_3$].$3H_2O$	$C_{20}H_{22}MnN_2O_{15}S$	617	39.31 (38.91)	3.40 (3.59)	4.79 (4.54)	8.90 (833)	15
[(HL)Fe (SO_4) $(H_2O)_3$] .$3H_2O$	$C_{20}H_{22}FeN_2O_{15}S$	618	39.26 (38.85)	3.39 (3.59)	4.73 (4.53)	9.03 (9.35)	20.50
[(HL) Ni $(OAc)_2(H_2O)_2$]. $3H_2O$ $O)_2$].$3H_2O$	$C_{24}H_{26}N_2NiO_{14}$	625	46.11 (46.09)	4.19 (4.14)	4.48 (4.45)	9.39 (9.46)	12.10
[(HL)Cu $(Cl)_2(H_2O)_2$].$2H_2O$	$C_{20}H_{20}C_{l2}CuN_2O_{10}$	582	41.21 (41.15)	3.46 (3.19)	4.81 (4.64)	10.90 (11.01)	11.00
[(HL)Zn (SO_4) $(H_2O)_3$].$3H_2O$	$C_{20}H_{22}N_2O_{15}SZn$	627	38.56 (38.26)	3.35 (3.53)	4.72 (4.46)	10.41 (10.84)	12.60

* $ohm^{-1}cm^2mol^{-1}$

4.1.2 IR Spectra

The mode of bonding between the ligand (HL) and its Mn(II), Fe(III), Ni(II), Cu(II) and Zn(II) metal complexes is determined by studying their IR spectra. The IR spectrum of the free ligand (HL) showed bands in the 3600-3340 and 3330-2650cm^{-1} ranges, commensurate the presence of two types of intra- and intermolecular hydrogen bonds of OH and NH groups with carbonyl group [10]. The higher frequency band is associated with a weaker hydrogen bond while, the medium band appeared at 3123 cm^{-1} is assigned to υ (NH) group [11]. The $\upsilon_{(NH)}$ group in the IR spectra of the complexes appeared at lower frequency side compared to this of the free ligand indicating that, this group is involved in the coordination to the metal ion [12]. The bands appeared at 1512, 1460, 760 and 710 cm^{-1} range, are assigned to υ (Ar) vibration [13]. By comparing the IR spectra of the complexes with that of the free ligand, it is clear that the $\upsilon_{(C=O)}$ amide complexes appeared at 1630-1610 cm-1 range indicating that, the amide group is not involved in the coordination to the metal ion [14]. In Ni acetate complexes, band were observed at 1576-1340 cm^{-1} range suggesting the coordination of acetate group in this complex as a monodentate, fashion [15]. The sulphato complexes Mn, Fe and Zn showed bands at 1277,1244 and 1275 cm^{-1} respectively assigned to monodentate sulphate group [16]. Cu(II) complex showed bands at 453-451cm^{-1} which is assigned to the $\upsilon_{(M-Cl)}$. In all complexes new two sets of bands are appeared within the ranges (469-617 cm-1) and (419-587 cm-1) due to the stretching vibrations $\upsilon_{(M-O)}$ and $\upsilon_{(M-N)}$ respectively. Accordingly, the mode of bonding in these complexes can be represented by the following scheme

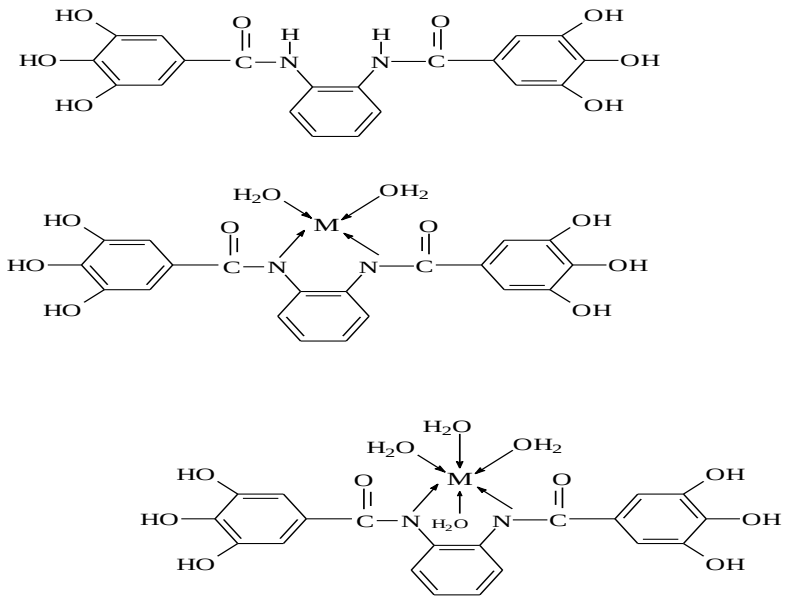

Table 2 IR Frequencies of the bands (cm^{-1}) of the ligand [HL], (1) and its Mn(II), Fe(III), Ni(II), Cu(II) and Zn(II) metal complexes

Comp.	ν (H2O)	ν(OH)	υ(H-bonding)	ν(NH)	ν(C=O) carb	ν SO4	ν(M-O)	υ(M-N)
(HL)	-	3442, 1385	(3537-3418), (3031-2360)	3290	1604	-	-	-
Cu(II)	(3455-3331), (3282-3190)	3412, 1459	(3509-3228), (3069-2360)	3282	1628	-	562	539
Mn(II)	(3463-3394), 3293-3198)	3499, 1384	(3150-3200), (3190-2926)	3330	1633	(1244,1078,616)	469	448, 419
Ni(II)	(3567-3310), (3327-3222)	3441, 1401	(3130-3072), (2970-2860)	3303	1798	(1460,1278)	617	587
Fe(III)	(3571,3417), (3211-3177)	3543, 1322	(3732-3136), (3089-2334)	3383	1637	(1275,1123,1077)	528	447
Zn(II)	(3574-3304), (3135-3099)	3385, 1462	(3620-3104), (3077-2335)	3236	1745	(1320,1277)	528	453

4.1.3 Mass Spectra

The mass spectra of some selected complexes were performed for further support of their molecular structure. The molecular ion peak (m/z; amu) are cited in Table (3) with the corresponding assignment.

Table 3 Mass spectral data (Molecular ion peak; m/z; amu) for some selected complexes

Complex	Mole. ion peak m/z	Assignment	Mole. ion peak m/z	Assignment
Free ligand	76 181 304	C_6H_4, $C_{12}H_5O_2$ $C_{14}H_8O_8$	335 374 400 412	$C_{14}H_{11}O_8N_2$ $C_{17}H_{16}O_8N_2$ $C_{19}H_{16}O_8N_2$ $C_{20}H_{16}O_8N_2$ (F.Wt
$[(HL)Fe(SO_4)(H_2O)_3].3H_2O$	116 135 168 248	$C_3H_2O_2NS$ $C_3H_5O_3NS$ $C_4H_{12}O_3N_2S$ $C_6H_{12}O_3N_2SFe$	325 386 512 618	$C_8H17_6N_2SFe$ $C_9H_{18}O_9N_2SFe$ $C_{18}H_{20}O_{10}N_2SFe$ $C_{20}H_{22}O_{15}N_2SFe$(F.Wt)
$[(HL)Ni(OAc)_2(H_2O)_2].3H_2O O)_2].3H_2O$	113 156 183 221 345	$C_4H_3O_3N$ $C_6H_6O_4N$ $C_7H_6O_5N$ $C_{10}H_7O_5N$ $C_{11}H_{13}O_8NNi$	395 445 495 625	$C_{14}H_{13}O_8N_2Ni$ $C_{16}H_{23}O_9N_2Ni$ $C_{16}H_{25}O_{12}N_2Ni$ $C_{24}H_{26}O_{14}N_2Ni$ (F.Wt)
$[(HL)Cu(Cl)_2(H_2O)_2].2H_2O$	191 205 267 301	$C_5H_2O_5NCl$ $C_6H_4O_5NCl$ $C_8H_{10}O_7NCl$ $C_8H_{14}O_8N_2Cl$	413 430 439 582	$C_{13}H_{15}O_9N_2Cl$ $C_{14}H_{20}O_9N_2Cl_2$ $C_{14}H_{20}O_9N_2Cl_2Cu$ $C_{20}H_{20}O_{10}N_2Cl_2Cu$(F.Wt)

4.1.4 Thermal Analysis (DTA And TGA)

Thermal methods of analysis open a new possibility for the investigation of metal complexes. The degradation steps of the samples can be followed up and the different degradation fragments can be estimated in the light of molecular structure of the complexes [20]. The thermogravimetrical behavior of the complex $[(HL)Cu(Cl)_2(H_2O)_2].2H_2O$ as an example is studied and its thermogram is shown in Fig. (1). Inspection of the TG – DT curves shows that the complex degrades thermally within the temperature range 30–800^oC through three main steps:

i. Dehydration of physically adsorbed and coordinated water molecules from the coordination sphere takeing place at the temperature of 50 ^oC.
ii. The unhydrated complex begins to decompose thermally through the second step at 317.11 ^oC leading to evolution of N_2 and CO_2 gases, finally
iii. Fully thermal decomposition takes place through the third step started at 600.02^oC leading to CuO as final product.

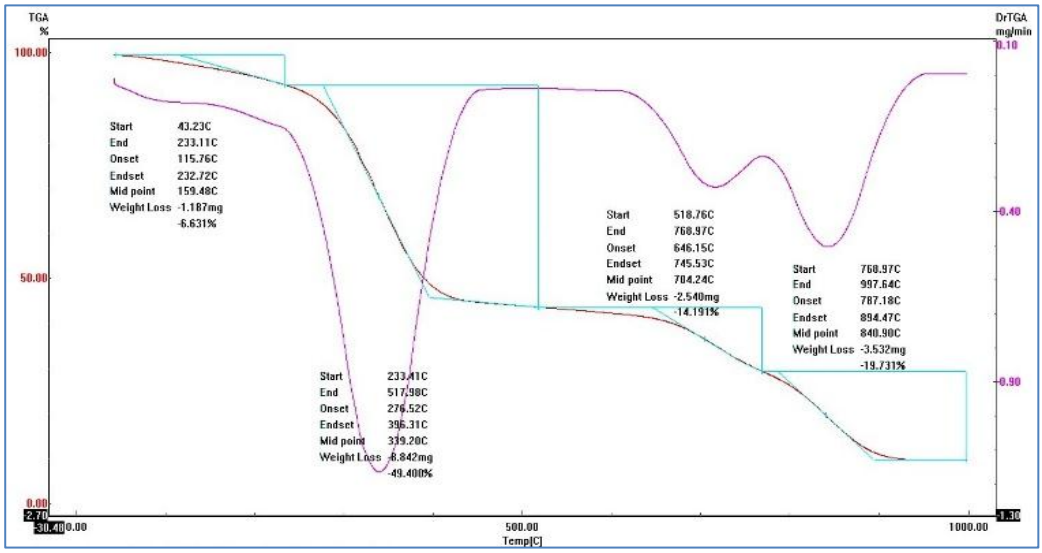

Fig. 1 Thermogram of the complex [(HL)Cu $(Cl)_2(H_2O)_2$].$2H_2O$

4.1.5 ^{1}H-NMR Spectra

The ^{1}H-NMR spectrum of the free ligand (HL) is measured in deutrated DMSO and compared to its [(HL)Zn (SO_4) $(H_2O)_3$].$3H_2O$ complex in the same solvent (***c.f.*** Fig.$2_{a,b}$). The spectrum of the ligand showed a singlet signal at δ = 9.2 ppm assigned to proton of hydroxyl group. The chemical shift which appeared at δ = 7.1 ppm is attributed to the proton of NH attached to (CH- of aromatic ring); (CO-NH-Ar-). A set of signals appeared as multiples in the 6.3-6.9 ppm range, corresponding to protons of aromatic ring [26]. By comparison the ^{1}HNMR of the ligand and the spectrum of the Zn complex, signal was observed as a singlet at 10 ppm characteristic to the OH group indicating that the ligand found in the protonated form. In addition, there is a significant downfield shift of the NH attached to (CH- of aromatic ring); (C=N-Ar-) proton signal relative to the free ligand clarified that, the metal ions are coordinated to the amide nitrogen atom. This shift may be due to the formation of a coordination bond (N→M) [27].

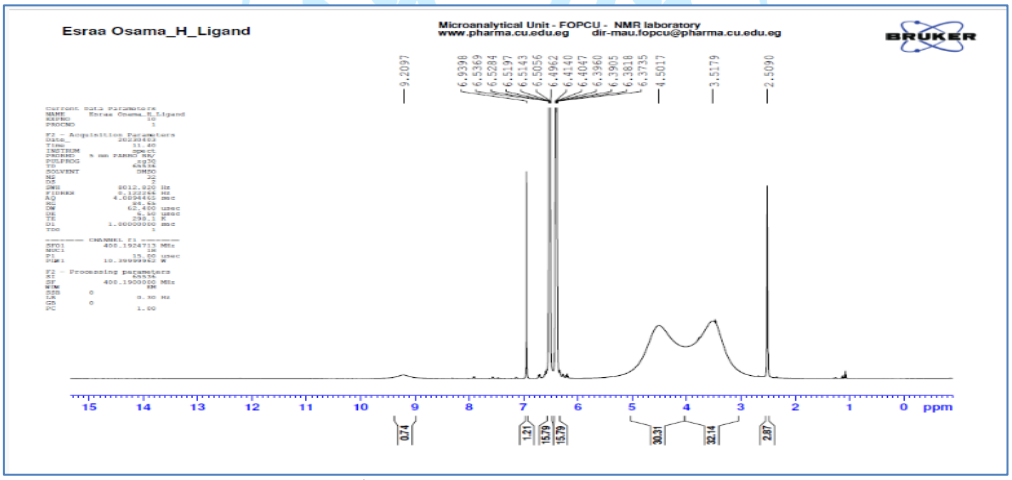

Fig. 2a ^{1}H- NMR spectra of the free ligand

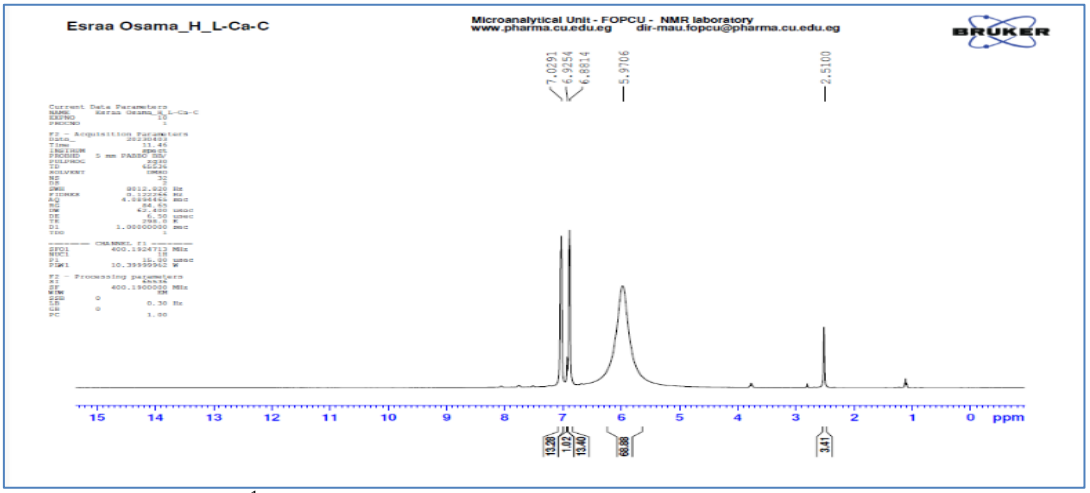

Fig. 2b ^{1}H- NMR spectra of the [(HL)Zn (SO_4) $(H_2O)_3$].$3H_2O$ complex

4.1.6 X-Ray Diffraction (XRD) Spectroscopy

Powder XRD pattern of the Cu (II) Ni(II) complexes were recorded in the range 2θ = 20–80 (***c.f.*** Fig. $3_{a,b}$). The XRD patterns of the show well defined crystalline peaks indicating their crystalline nature. The average crystallite size of each complex was estimated the modified form Scherer's formula [RRR]: $d_{XRD} = 0.9\lambda/\beta\ (\cos\theta)$

where 'λ' is the wavelength, 'β' is the full width at half maxima and 'θ' is the diffraction angle. The XRD reveal that the average crystallite sizes are within the ranges of 5.9-17.3nm, and 5.15-15.6 nm respectively suggesting that the Complexes are nanocrystalline [43].

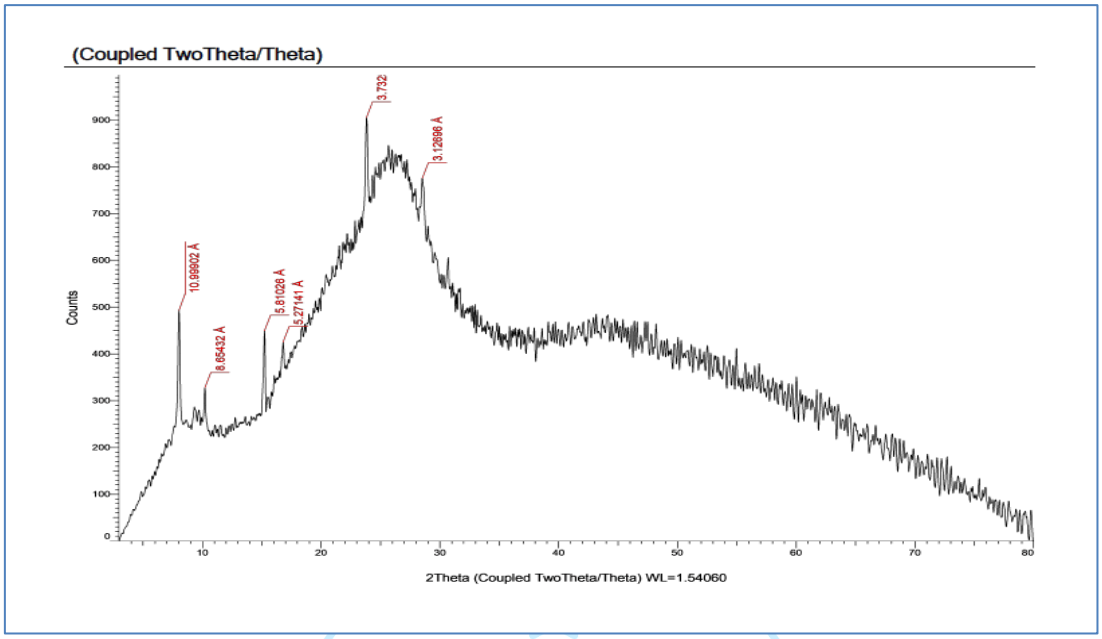

Fig. 3a XRD pattern of the Cu(II) complex

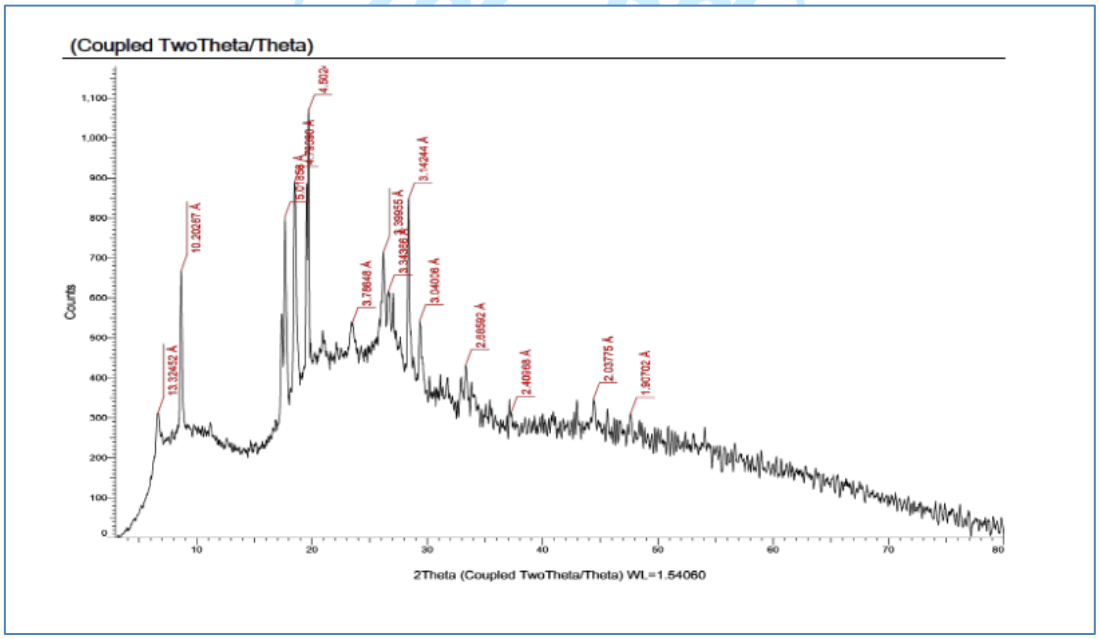

Fig. 3b XRD pattern of the Ni(II) complex

5. Biological Activity

5.1 Toxicity Study

Toxicity studies of Iron (II), copper (II) and zinc (II) complexes were done. The complexes were dissolved in DMSO and then diluted by sterile saline 0.9 % NaCl in a maximum concentration of 0.2% by volume to be able to be injected intra peritoneal.The LD_{50} for all tested complexes nanoparticles were devoid of any acute toxicity in rats when given the selected different doses by intra-peritoneal route [50].

5.2 Biochemical Analyses

The results of the present study (cited in Table 4) showed that the measurements of liver functions (AST, ALT and albumin) and renal functions (B.Urea & S.Creatinine) showed no significant differences between treated groups of rats and the control group, which proves that there are no toxic side effects for the tested complexes.

Table 4 Statistical analysis (ANOVA) for liver and kidney function tests in the different groups

Parameters	Control	Cu(II) complex	Zn(II) complex	Fe(II) complex
AST (U/l)	97.431 ±12.152	95.334 ±14.291	99.471 ±11.208	101.083 ±14.291
ALT (U/l)	37.527 ±4.953	36.925 ±5.011	39.144 ±6.152	39.991 ±5.853
Alb (g/dl)	4.604 ±0.627	4.770 ±0.539	4.622 ±0.207	4.382 ±0.811
B. Urea (mg/dl)	32.146 ±5.104	34.091 ±2.693	31.892 ±3.007	34.350 ±4.921
S. Creatinine (mg/dl)	0.499 ±0.095	0.502 ±0.117	0.524 ±0.162	0.537 ±0.189

ANOVA: analysis of variance; AST: aspartate aminotransferase; ALT: alanine aminotransferase; Alb: albumin; B.Urea: Blood urea; S.Creatinine: Serum creatinine. Each value is represented as mean ± SD. SD: standard deviation. Data with different superscripts are significantly different at $p \leq 0.05$.

5.3 Hematological analysis

The results of the analysis of some hematological parameters (Hb, RBCs, TLC and platelets counts) cited in Table 5 showed no significant changes between the control group and the treated groups by the chosen complexes as follow:

Table 5 Statistical analysis (ANOVA) for hematological tests in the different groups

Parameters	Control	Cu(II) complex	Zn(II) complex	Fe(II) complex
Hb (g/dl)	16.51 ±5.014	16.304 ±2.592	16.242 ±3.181	16.859 ±4.660
RBCs (X 106/cmm)	6.611 ±1.635	6.447 ±1.053	6.143 ±1.892	6.934 ±1.246
TLC (X 103/cmm)	10.527 ±2.075	11.025 ±1.882	9.992 ±2.631	10.856 ±1.684
Plts (X 103/cmm)	701.152 ±44.632	611.391 ±62.952	668.661 ±41.084	766.054 ±50.569

ANOVA: analysis of variance; Hb: Hemoglobin concentration; RBCs: Red blood corpuscles count; T.L.C: Total leucocytic count; Plts: Platelets count. Each value is represented as mean ± SD. SD: standard deviation Data with different superscripts are significantly different at $p \leq 0.05$.

5.4 Molecular Docking Studies on Anti-Prostate Cancer

This study aimed to use the 6XXO protein (prostate cancer protein) for the discovery of new targeted therapy. To determine the most likely compound that can bind to the 6XXO protein, we docked the modeled 6XXO 3D structure against the ligand (HL) and some of its complexes using Moldock score. Protein basic local alignment search tool (BLASTp), multiple sequence alignment (MSA), and phylogenetics were further carried out to analyze the diversity of this marker and to determine its conserved domains as suitable target regions. Two promising drug candidates (ligands) were identified.The docked ligand with 6XXO which is responsible for prostate cancer Fig.(4) shows electrostatic and hydrogen bond between ligand with receptor interaction distances of ≤ 3.50 Ao indicating the presence of typical real bonds which means high binding affinity. For example, the nearest interaction is observed via H-donors with 6XX0 (2.85 Ao) and ligand with Moldock score 27199 and plants score 222.852, an excellent binding sites of designed drug with different amino acids (Pro 41 and Glu 89) were observed which demonstrating their ability of inhibition of prostate cancer, Fig. (5).

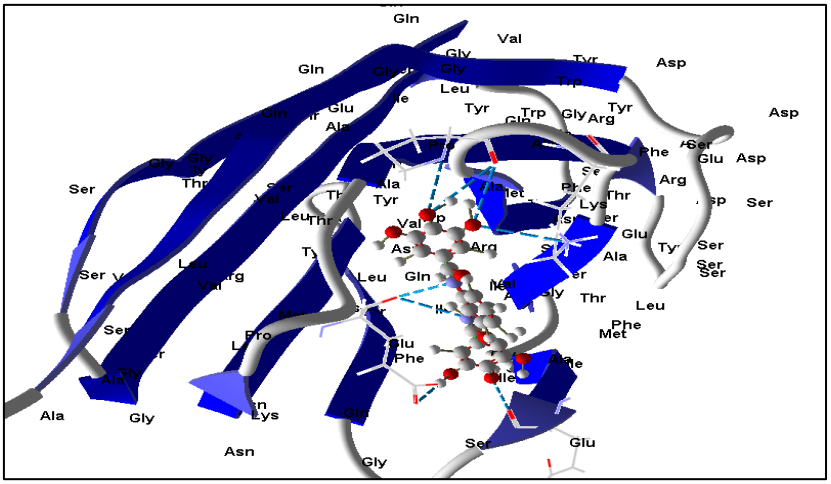

Fig. 4 Virtual Molecular docking of the best docked of ligand; HL (1) with 6XXO protein

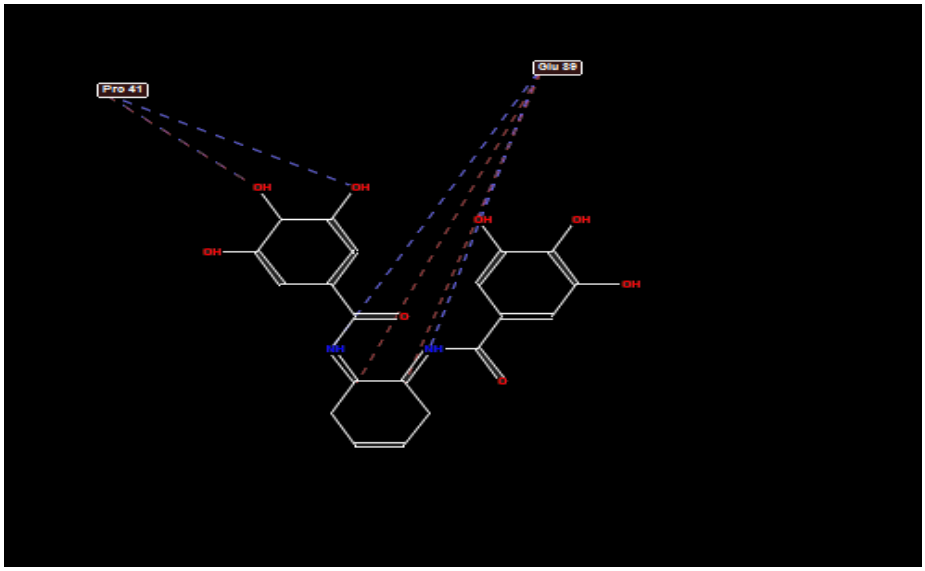

Fig. 5 2D structure of Molecular docking of ligand; HL (1) with 6XXO protein

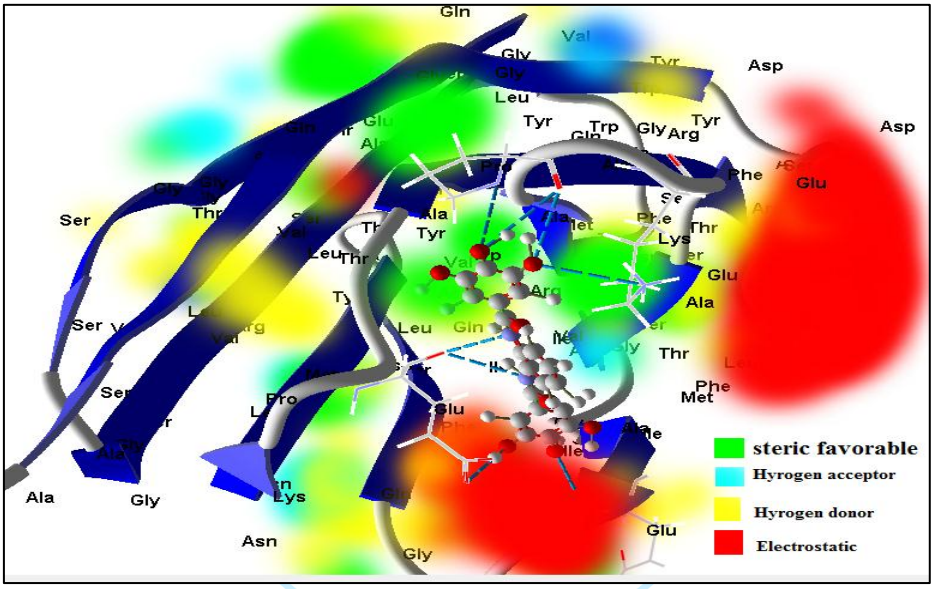

Fig. 6 Energy map of docked ligand; HL (1)

5.5 Cu(II) Acetate Complex $[(HL)Cu(OAc)_2(H_2O)_2].2H_2O$ $C_{24}H_{26}CuN_2O_{14}$

When Cu(II) complex is docked with 6XXO prostate cancer prostate; Fig. (7) it shows a higher electrostatic and hydrogen bond between complex and receptor than ligand; Fig. (8). The nearest interaction is observed *via* H-donors with 6XX0 (2.56A^o) and copper metal which indicates the presence of typical real bonds which meaning high binding affinity with Moldock score 65630.7 and plants score 1567. The binding sites of designed drug with different amino acids (Glu 44,Glu 46,Glu 89, Arg 38, Lys 43and Ala 40) were observed which demonstrating their higher inhibition than ligand due to highest binding energy.

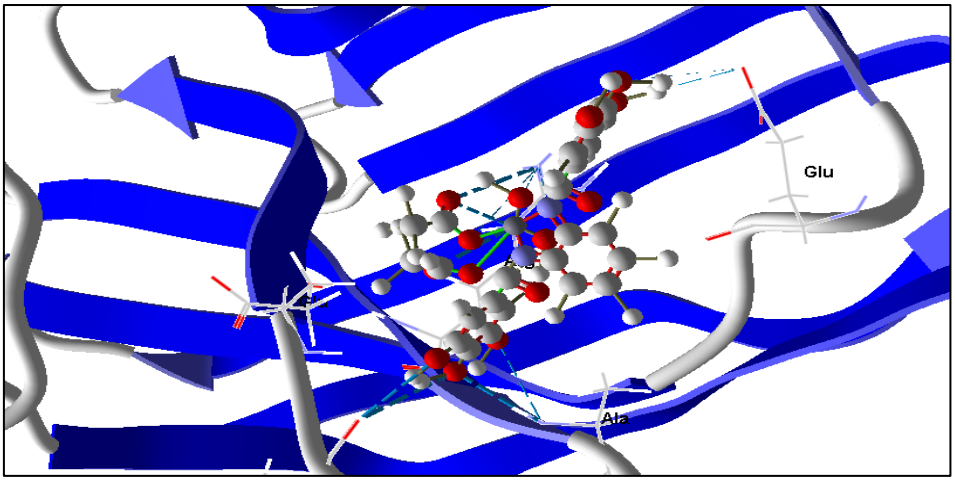

Fig. 7 Virtual Molecular docking of the best docked Cu(II); complex (2) with 6XXO protein

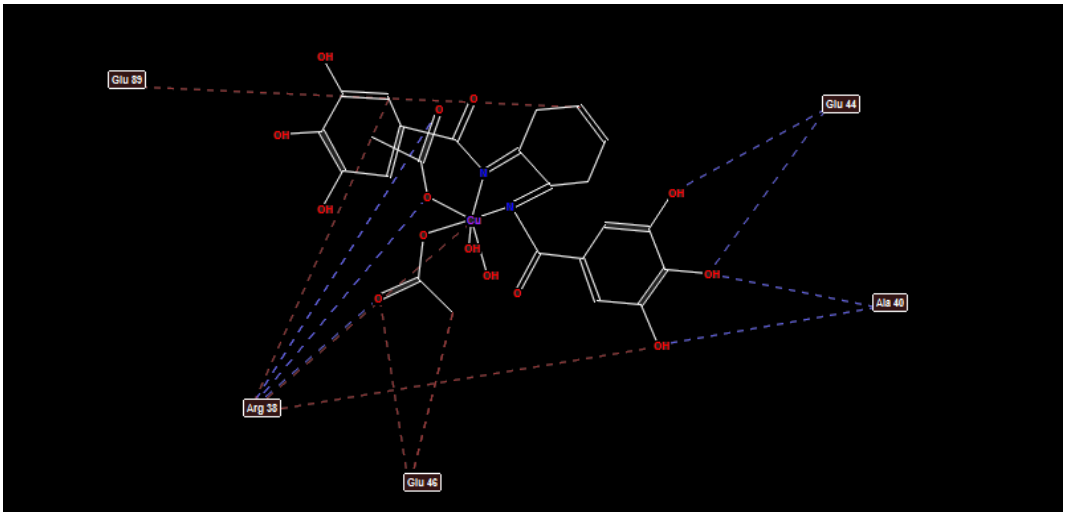

Fig. 8 2D structure of Molecular docking of Cu(II); complex (2)with 6XX0 protein

5.6 Ni(II) acetate complex: [(HL) Ni $(OAc)_2(H_2O)_2$].$3H_2O$ $C_{24}H_{26}N_2NiO_{14}$

The designed drug (Nikel acetate metal complex) is docked with 6XXO prostate cancer prostate. Fig. (9) shows a higher electrostatic and hydrogen bond between complex and receptor than ligand. The nearest interaction is observed *via* H-donors with 6XX0 (2.62A) and (Ni metal) which indicates the presence of typical real bonds which means high binding affinity with Moldock score 53670 and plants score 1365 , the binding sites of designed drug with different amino acids (Glu 44, Glu 89, Arg 38, and Ala 40) were observed which demonstrating their higher inhibition than ligand due to highest binding energy.

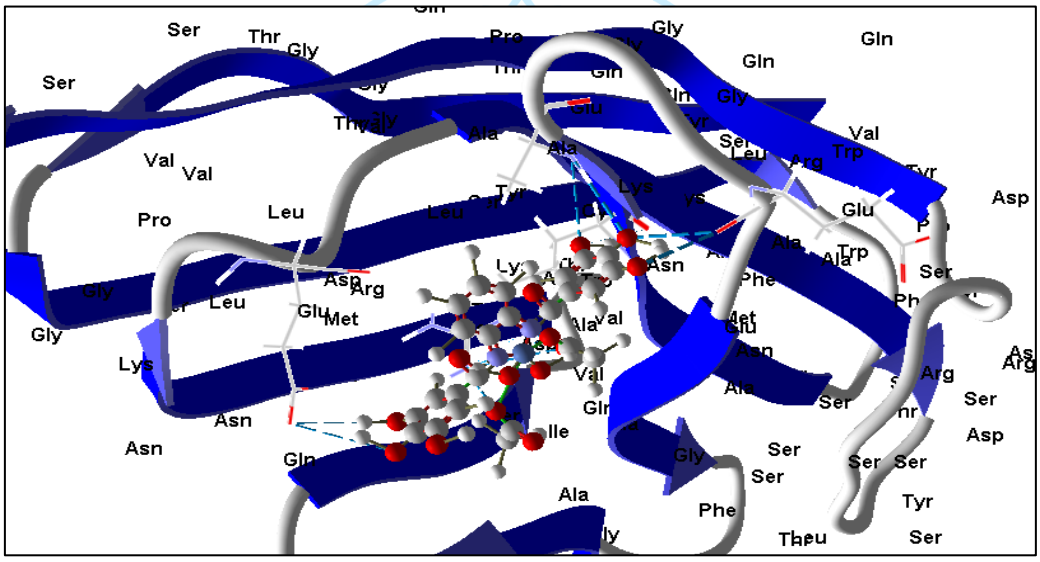

Fig. 9 Virtual Molecular docking of the best docked Ni(II); complex (7) with 6XXO protein

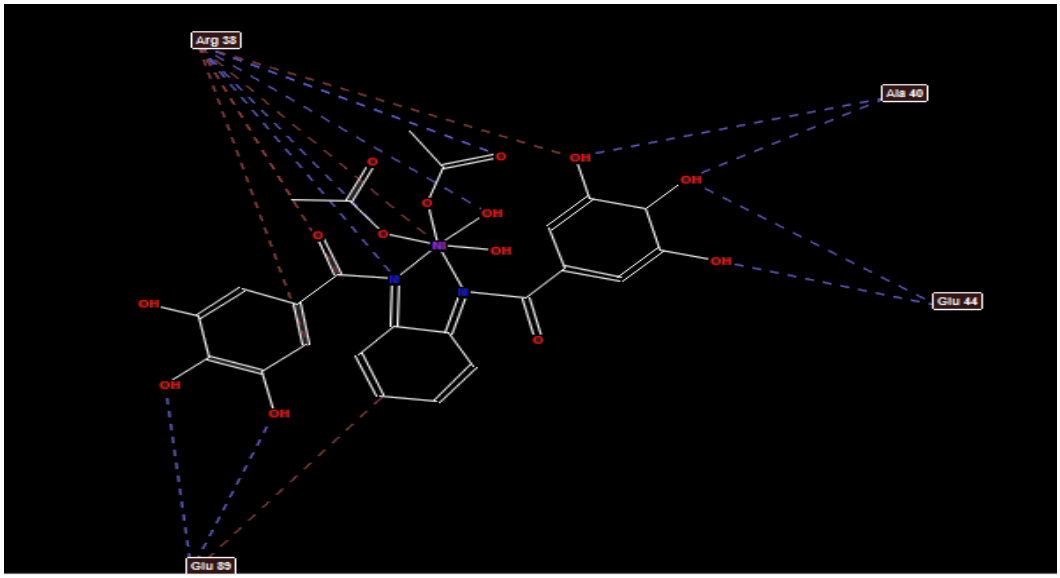

Fig. 10 2D structure of Molecular docking of Ni(II); complex (7) with 6XX0 protein

5.7 Mn-acetate complex (5): $[(HL)Mn(OAc)_2(H_2O)_2].2H_2O$ $C_{24}H_{26}MnN_2O_{14}$

The designed drug (Mn- acetate metal complex) is docked with 6XXO prostate cancer prostate Fig. (20) shows a higher electrostatic and hydrogen bond between complex and receptor than ligand. The nearest interaction is observed *via* H-donors with 6XX0 (2.62A) and (copper metal complex) which indicates the presence of typical real bonds which means high binding affinity With Moldock score 58606 and plants score 1243 , the binding sites of designed drug with different amino acids (Glu 44, Glu 89, Arg 38, and Ala 40) were observed which demonstrating their higher inhibition than ligand due to highest binding energy.

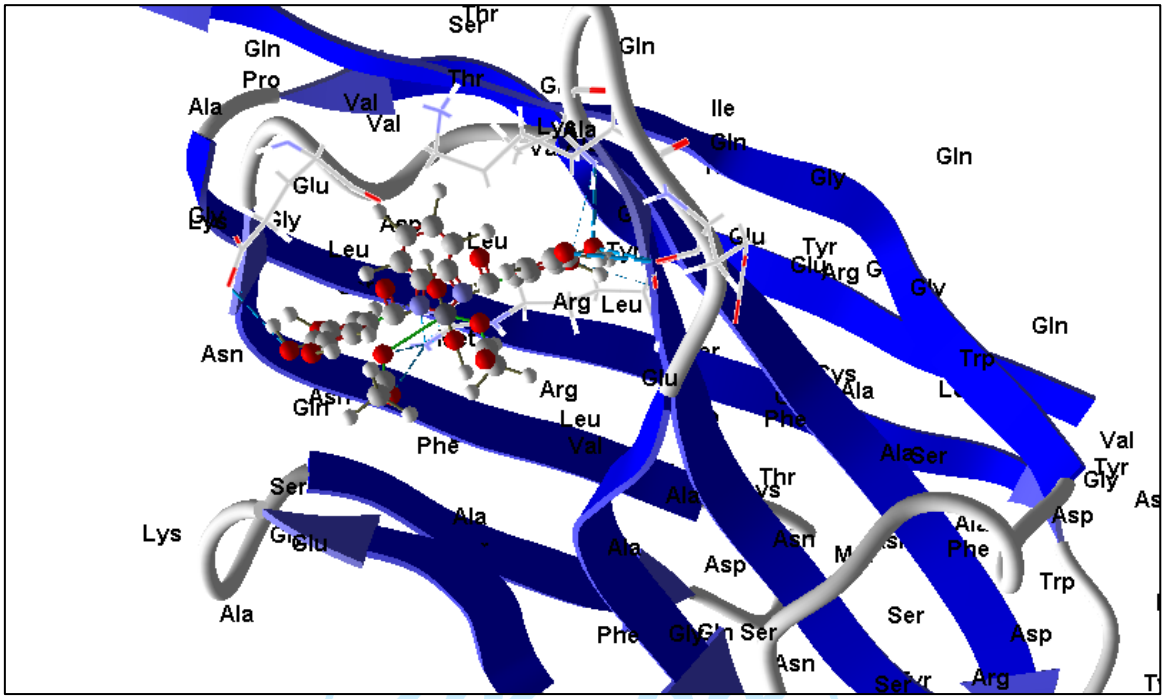

Fig. 11 Virtual Molecular docking of the best docked Mn(II); complex (5) with 6XXO protein

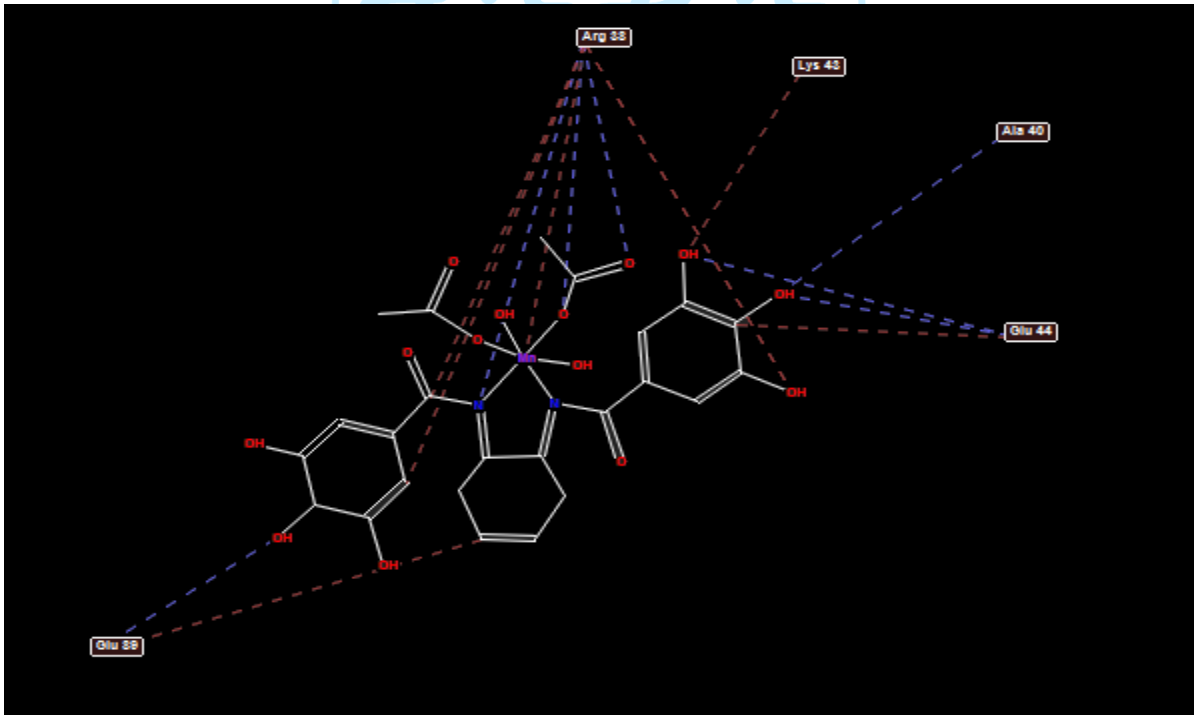

Fig. 12 2D structure of Molecular docking of Mn(II); complex (5) with 6XX0 protein

5.8 Cu-Sulfate complex (3): $[(HL)Cu(SO_4)(H_2O)_3].2H_2O$ $C_{20}H_{22}CuN_2O_{15}S$

The designed drug (Cu- sulfate metal complex) is docked with 6XXO prostate cancer prostate Fig. (13) shows an higher electrostatic and hydrogen bond between complex and receptor than ligand. The nearest interaction is observed *via* H-donors with 6XX0 (2.59A) and (copper metal complex) which indicates the presence of typical real bonds which means high binding affinity With Moldock score 71604 and plants score 1490 , the binding sites of designed drug with different amino acids (Glu 44, Arg 38, and Ala 40) were observed which demonstrating their higher inhibition than ligand due to highest binding energy.

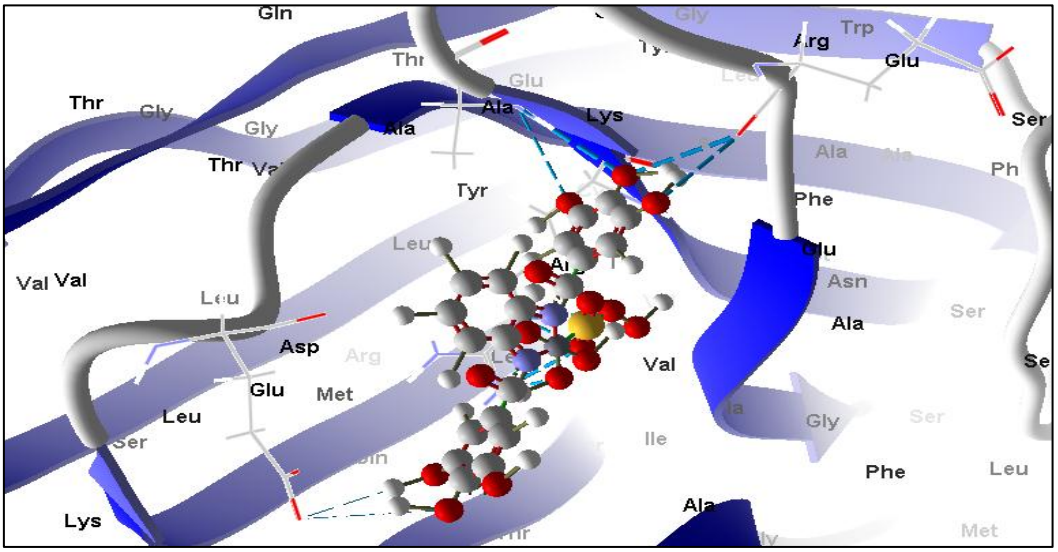

Fig. 13 Virtual Molecular docking of the best docked Cu(II); complex (3) with 6XXO protein

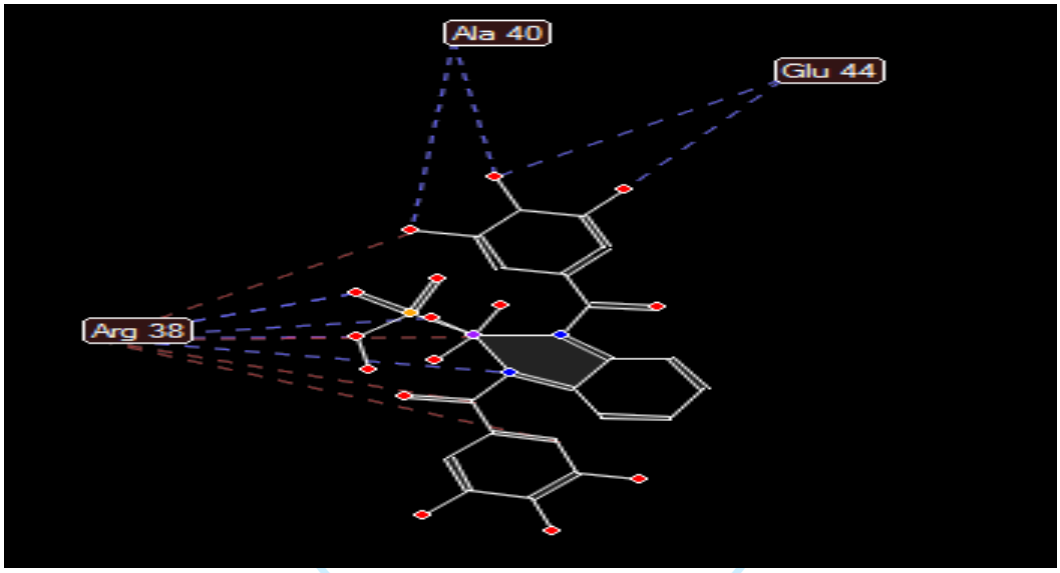

Fig. 14 2D structure of Molecular docking of Cu(II); complex (3) with 6XX0 protein

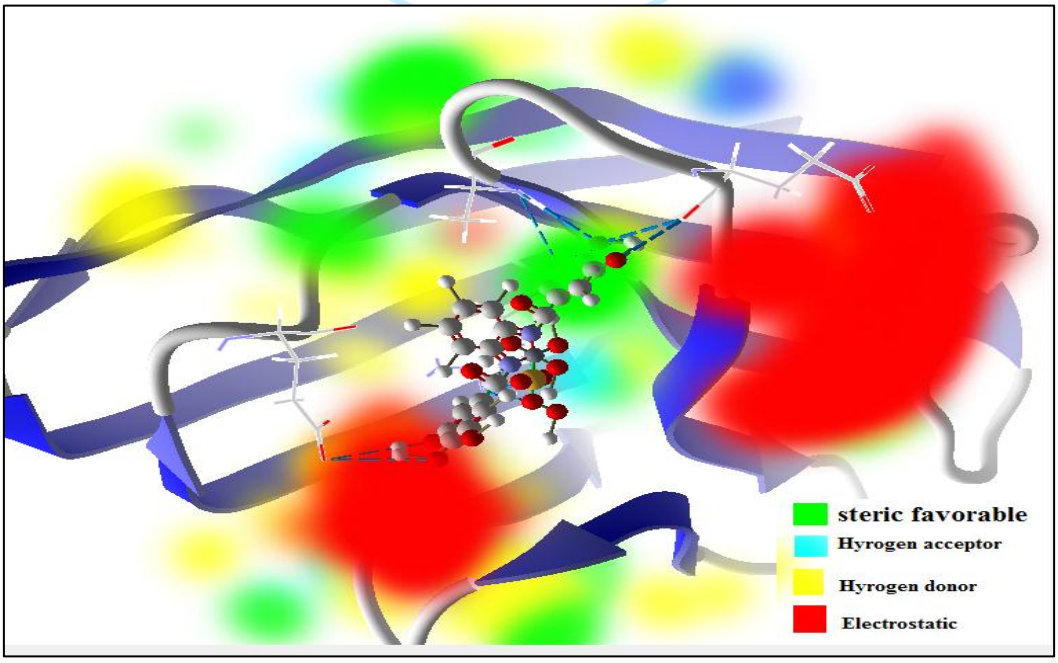

Fig. 15 Energy map of docked ligand**;** HL (1)

From above data it can be concluded that Cu-Sulfate complex> copper acetate metal> Mn-acetate complex> Mn- acetate> Ni- acetate towards inhibition of prostate cancer.

6. Conclusion

Biologically active N, N'-(1,2-phenylene) bis-(3,4,5-trihydroxybenzamide) ligand and its metal complexes Mn(II), Fe(III), Ni(II), Cu(II) and Zn(II) have been prepared and characterized by various spectroscopic techniques (XRD,IR,^{1}H-NMR and Mass Spectroscopy) and also have been characterized by elemental and thermal analysis (TGA and DTA). The cytotoxic activity of some solid complexes against experimental animals (Albino rats) prostate cell cancer was extensively studied and expressed as lethal dose 50 (LD_{50}). The acute intra-peritoneal toxicity of the chosen complexes was done using 21 experimental rat animals and molecular docking studies against prostate cancer cell line (PC-3) had been done and compared to the practical data obtained and we found that Cu-Sulfate complex> copper acetate metal> Mn-acetate complex> Mn- acetate> Ni- acetate towards inhibition of prostate cancer.

Author's Contributions

ASE and MHA designed the study and performed the complexes synthesis. AMA, MHA, EOA and AGA performed most of the experiments (Biochemical and hematological analyses), analyzed and interpreted the data. MHA performed and interpreted the molecular docking studies. MHA, AMA and EAM wrote the first version of the manuscript. All authors reviewed and approved the final version of the manuscript.

Conflict of Interest

The authors have declared no conflict of interest.

Funding

The author(s) received no financial support for the research or authorship.

Ethics Approval

This study was performed after getting permission from the Institutional Animal Ethical Committee, Menoufia University, Egypt (approval ID: MUFS/F/CH/1/23).

References

1. Abdul Ghafor, A. A. H. (2020). Toxicity assessment of gallic acid loaded graphene oxide (GAGO) nano-formulation in zebrafish (Danio rerio) embryos. Pertanika Journal of Science & Technology, 28, 311–326.
2. Aborehab, N. M., Elnagar, M. R., & Waly, N. E. (2021). Gallic acid potentiates the apoptotic effect of paclitaxel and carboplatin via overexpression of Bax and P53 on the MCF-7 of Bax and P53 on the MCF-7 line. Journal of Biochemical and Molecular Toxicology, 35, e22638. https://doi.org/10.1002/jbt.22638
3. Dashtbani-Roozbehani, A., & Brown, M. H. (2021). Efflux pump mediated antimicrobial resistance by staphylococci in health-related environments: Challenges and the quest for inhibition. Antibiotics, 10, 1502. https://doi.org/10.3390/antib iotic s1012 1502
4. Hossain, M. A., Park, H.-C., Park, S.-W., Park, S.-C., Seo, M.-G., Her, M., & Kang, J. (2020). Synergism of the combination of traditional antibiotics and novel phenolic compounds against Escherichia coli. *Pathogens, 9*, 811. https://doi.org/10.3390/patho gens9 100811
5. Keyvani-Ghamsari, S., Khorsandi, K., & Gul, A. (2020). Curcumin effect on cancer cells' multidrug resistance: An update. Phytotherapy Research, 34, ptr.6703. https://doi.org/10.1002/ptr.6703
6. Lin, T.-H., Wu, C.-C., Tseng, C.-Y., Fang, J.-H., & Lin, C.-T (2022). Effects of gallic acid on capsular polysaccharide biosynthesis in Klebsiella pneumoniae. Journal of Microbiology, Immunology, and Infection., 55, 1255–1262.
7. Manso, T., Lores, M., & de Miguel, T. (2021). Antimicrobial activity of polyphenols and natural polyphenolic extracts on clinical isolates. *Antibiotics*, *11*, 46. https://doi.org/10.3390/antib iotic s11010046
8. Rana, A.; Samtiya, M.; Dhewa, T.; Mishra, V.; Aluko, R.E. Health benefits of polyphenols: A concise review. J. Food Biochem. 2022, 46, e14264. [CrossRef] [PubMed]
9. Tan, S.; Hua, X.; Xue, Z.; Ma, J. Cajanin Stilbene Acid Inhibited Vancomycin-Resistant Enterococcus by Inhibiting Phosphotransferase System. Front. Pharmacol. 2020, 11, 473. [CrossRef]
10. Selvaraj, S., Rajkumar, P., Kesavan, M., Gunasekaran, S., & Kumaresan, S. (2019). Experimental and theoretical analyzes on structural and spectroscopic An properties of monomer and dimeric form of (S)-Piperidine-2-Carboxylic acid: attempt on medicinal plant. Vibrational Spectroscopy, 100, 30-39.
11. El-Ghamry, M. A., Elzawawi, F. M., Aziz, A. A. A., Nassir, K. M., & Abu-El-Wafa, S. M. (2022). New Schiff base ligand and its novel Cr (III), Mn (II), Co (II), Ni (II), Cu (II), Zn (II) complexes: Spectral investigation, biological applications, and semiconducting properties. Scientific Reports, 12(1), 17942.
12. Begum, N., Mustaq, S., Aziz, S. S., & Arifuddin, M. (2021). Indian Journal of Advances in Chemical Science. Indian Journal of Advances in Chemical Science, 9(3), 218-225.
13. El-Tabl, A. S., Ismail, A. E. H., Abd EL-Wahed, M. M., Sayed Ahmed, R. A., & Ashour, A. M. (2022). Novel nano-metal complexes of modified aspirin as future antimicrobial agents. International Journal of Pharmaceutical Research (09752366), 14(1).

14. El-Tabl, A. S., Abd-El Wahed, M. M., Sayed Ahmed, R. A., Alhalib, A. A. A., & Ashour, A. M. (2022). Physico-chemical Characterization and Estimation of Antimicrobial Activity of Modified Aspirin in the form of Nano-organometallic Compounds. Chemical Science International Journal, 31(3), 11-37.
15. El Tabl, A. S., Abd-El Wahed, M. M., Ashour, A. M., Aly, A. A., Abu-Setta, M. H.H. (2023). Recent advances in metal complexes of new multifunctional ether ligand as potential anti-breast cancer agents. European Chemical Bulletin, 12 (5), 1436-1463.
16. Ali, S. G., El Tabl, A. S., Shabana, A. A., Abd-El Wahed, M. M., Ashour, A. M., Abu-Setta, M. H.H. & Elzaref A. S. (2023). Recent advances in metal complexes of new multifunctional ether ligand as potential anti-breast cancer agents. European Chemical Bulletin, 12 (5), 1464-1514
17. Liu, Zeyu, Tian Lu, and Qinxue Chen. "An sp-hybridized all-carboatomic ring, cyclo [18] carbon: Electronic structure, electronic spectrum, and optical nonlinearity." Carbon 165 (2020): 461-467.
18. Griesar, K., & Haase, W. (2023). Magnetic properties of transition-metal-containing liquid crystals. In Magnetic properties of organic materials (pp. 325-344). Routledge.
19. Melendez-Rodriguez, B., Torres-Giner, S., Zavagna, L., Sammon, C., Cabedo, L., Prieto, C., & Lagaron, J. M. (2021). Development and characterization of electrospun fiber-based poly (ethylene-co-vinyl alcohol) films of application interest as high-gas-barrier interlayers in food packaging. Polymers, 13(13), 2061.
20. Dilissen, N., Vleugels, J., Vermeiren, J., García-Baños, B., Marín, J. R. S., & Catalá-Civera, J. M. (2023). Temperature dependency of the dielectric properties of hydrated and ordinary Portland cement and their constituent phases at 2.45 GHz up to 1100 C. Cement and Concrete Research, 165, 107067.
21. Xie, B., Chen, J., Chen, J., Ma, C., Zhao, L., & Tchameni, A. P. (2023). Novel thermo-associating polymer/silica nanocomposite as a temperature-resistant rheology modifier for bentonite-free water-based drilling fluids. Geoenergy Science and Engineering, 222, 211426.
22. Vasile, B. S., Dobra, G., Iliev, S., Cotet, L., Neacsu, I. A., Surdu, V. A & Filipescu, L. (2021). Thermally activated Al (OH) 3 part II—effect of different thermal treatments. Ceramics, 4(4), 564-575.
23. Singh, N. K., Sharma, S., Krishnakumar, A., Choudhary, R. K., Kumbhar, A. A., Butcher, R. J., ... & Yadav, P. N. (2022). Exploration of anticancer potency of N (4) thiomorpholinyl isatin/5-haloisatin thiosemicarbazones on coordination to Cu2+ ion. Inorganic Chemistry Communications, 143, 109767.
24. Wang, L., Li, Z., Wu, Q., Huang, Z., Yuan, L., Chai, Z., & Shi, W. (2020). Layered structure-based materials: challenges and opportunities for radionuclide sequestration. Environmental Science: Nano, 7(3), 724-752.
25. Do Prado, M. V., González, B., Vicente, M. A., Trujillano, R., Nassar, E. J., Gil, A., & Ciuffi, K. J. (2023). Multifunctional heterogeneous catalysts: Tetrakis (pentafluorophenyl) porphinato] iron (III) immobilized on amine–functionalized Diatomaceous Earth for catalytic and adsorption applications. Journal of Environmental Chemical Engineering, 11(3), 109729.
26. Selvaraj, S., Rajkumar, P., Kesavan, M., Gunasekaran, S., & Kumaresan, S. (2019). Experimental and theoretical analyzes on structural and spectroscopic properties of monomer and dimeric form of (S)-Piperidine-2-Carboxylic acid: An attempt on medicinal plant. Vibrational Spectroscopy, 100, 30-39.
27. Ibrahim, H., Bala, M. D., & Friedrich, H. B. (2022). Poly-functional imino-N-heterocyclic carbene ligands: Synthesis, complexation, and catalytic applications. Coordination Chemistry Reviews, 469, 214652.
28. Pei, S., You, S., Ma, J., Chen, X., & Ren, N. (2020). Electron spin resonance evidence for electro-generated hydroxyl radicals. Environmental Science & Technology, 54(20), 13333-13343.
29. El-Tabl, Abdou S., Mohamed Tawfek Shaban, and Noran Mohamed Abd El-Wahed. "Novel metal complexes as antimicrobial agents, synthesis and spectroscopic characterization." Journal of Chemistry and Chemical Sciences 9.3 (2019): 74-108.
30. Barba, F. J., Roohinejad, S., Ishikawa, K., Leong, S. Y., Bekhit, A. E. D. A., Saraiva, J. A., & Lebovka, N. (2020). Electron spin resonance as a tool to monitor the influence of novel processing technologies on food properties. Trends in Food Science & Technology, 100, 77-87.
31. Delgado, F., & Lorente, N. (2021). A theoretical review on the single-impurity electron spin resonance on surfaces. Progress in Surface Science, 96(2), 100625.
32. Zhang, X., Wolf, C., Wang, Y., Aubin, H., Bilgeri, T., Willke, P., ... & Choi, T. (2022). Electron spin resonance of single iron phthalocyanine molecules and role of their non-localized spins in magnetic interactions. Nature Chemistry, 14(1), 59-65.
33. Chiappinelli, A., Mangiacotti, M., Tomaiuolo, M., Trotta, G., Marchesani, G., & Chiaravalle, A. E. (2019). Identification of X-ray-irradiated hazelnuts by electron spin resonance (ESR) spectroscopy. European Food Research and Technology, 245(10), 2323-2329.
34. King, G. E., Tsukamoto, S., Herman, F., Biswas, R. H., Sueoka, S., & Tagami, T. (2020). Electron spin resonance (ESR) thermochronometry of the Hida range of the Japanese Alps: validation and future potential. Geochronology, 2(1), 1-15.
35. Jiang, S., Xie, Y., Li, M., Guo, Y., Cheng, Y., Qian, H., & Yao, W. (2020). Evaluation on the oxidative stability of edible oil by electron spin resonance spectroscopy. Food chemistry, 309, 125714.

36. Hwang, J., Krylov, D., Elbertse, R., Yoon, S., Ahn, T., Oh, J., ... & Bae, Y. (2022). Development of a scanning tunneling microscope for variable temperature electron spin resonance. Review of Scientific Instruments, 93(9).
37. Moro, F., Ke, S., del Águila, A. G., Söll, A., Sofer, Z., Wu, Q., ... & Fanciulli, M. (2022). Revealing 2D Magnetism in a Bulk CrSBr Single Crystal by Electron Spin Resonance. Advanced Functional Materials, 32(45), 2207044.
38. Willke, P., Singha, A., Zhang, X., Esat, T., Lutz, C. P., Heinrich, A. J., & Choi, T. (2019). Tuning single-atom electron spin resonance in a vector magnetic field. Nano Letters, 19(11), 8201-8206.
39. Moro, F., Ke, S., del Águila, A. G., Söll, A., Sofer, Z., Wu, Q., ... & Fanciulli, M. (2022). Revealing 2D Magnetism in a Bulk CrSBr Single Crystal by Electron Spin Resonance. Advanced Functional Materials, 32(45), 2207044.
40. Gálvez, J. R., Wolf, C., Delgado, F., & Lorente, N. (2019). Cotunneling mechanism for all-electrical electron spin resonance of single adsorbed atoms. Physical Review B, 100(3), 035411.
41. Singamaneni, S. R., Martinez, L. M., Niklas, J., Poluektov, O. G., Yadav, R., Pizzochero, M., ... & McGuire, M. A. (2020). Light induced electron spin resonance properties of van der Waals CrX3 (X= Cl, I) crystals. Applied Physics Letters, 117(8).
42. Almagul, U., Shah, A., & Zhazira, B. (2020). Studies on Valued Components Extraction from Titanium-Magnesium Production Wastes. Journal of Advanced Research in Fluid Mechanics and Thermal Sciences, 75(3), 140-155.
43. Thakar, M. A., Jha, S. S., Phasinam, K., Manne, R., Qureshi, Y., & Babu, V. H. (2022). X ray diffraction (XRD) analysis and evaluation of antioxidant activity of copper oxide nanoparticles synthesized from leaf extract of Cissus vitiginea. Materials Today: Proceedings, 51, 319-324.
44. Relucenti, M., Familiari, G., Donfrancesco, O., Taurino, M., Li, X., Chen, R., ... & Selan, L. (2021). Microscopy methods for biofilm imaging: focus on SEM and VP-SEM pros and cons. Biology, 10(1), 51.
45. El-Tabl, A.S., Abd-El Wahed, M. M., Abu-Setta, M.H.H., El-Mahsarawy, A.I., & Ashour, A.M (2022). Cytotoxicity and antitumor activity of organometallic copper (II) Nano particles in a chemically induced hepatocellular carcinoma rat model. International Journal of Pharmaceutical Sciences and Research, Vol.14 (3): 1000-11
46. Parolini, M. (2020). Toxicity of the Non-Steroidal Anti-Inflammatory Drugs (NSAIDs) acetylsalicylic acid, paracetamol, diclofenac, ibuprofen and naproxen towards freshwater invertebrates: A review. Science of the Total Environment, 740, 140043.
47. Said, D. E., Amer, E. I., Sheta, E., Makled, S., Diab, H. E., & Arafa, F. M. (2022). Nano-Encapsulated Melatonin: A Promising Mucosal Adjuvant in Intranasal Immunization against Chronic Experimental T. gondii Infection. Tropical Medicine and Infectious Disease, 7(12), 401.
48. Neghab, M., Amiri, F., Soleimani, E., Yousefinejad, S., & Hassanzadeh, J. (2020). Toxic responses of the liver and kidneys following occupational exposure to anesthetic gases. EXCLI journal, 19, 418.
49. El-Shafey, A. A., El-Ezabi, M. M., Ouda, H. H., Hegazy, M. M., & Ibrahim, D. S. (2023). Effect of wheat germ oil on phenylhydrazine-induced toxicity in male albino rats. Egyptian Journal of Experimental Biology (Zoology), 19(1).
50. El Tabl, A., Abdel Wahed, M., El Assaly, M. M., & Ashour, A. (2021). Nano-organometallic complexes as therapeutic platforms against breast cancer cell lines;(in vitro study). Egyptian Journal of Chemistry, 64(3), 1627-1637.
51. Pfaller, M.A.; Burmeister, L.; Bartlett; Ghorab, M.A.; Rinaldi, M.G. J. Clin. Microbiol. 1988, 26, 1437-1441.
52. CLSI; Clinical and Laboratory Standards Institute, 2012, Twentieth informational supplement. M100-S22. Wayne: PA.
53. Mahmoud F. Abo-Ashour, Wagdy M. Eldehna, Riham F. George, Marwa M. Abdel-Aziz, Mahmoud M. Elaasser, Nagwa M. Abdel Gawad, Antima Gupta, Sanjib Bhakta, Sahar M. Abou-Seri (2018): Novel indole-thiazolidinone conjugates: Design, synthesis and whole-cell phenotypic evaluation as a novel class of antimicrobial agents. European Journal of Medicinal Chemistry 10/2018; 160., DOI:10.1016/j.ejmech.2018.10.008
54. Hany S. Ibrahim, Wagdy M. Eldehna, Hatem A. Abdel-Aziz, Mahmoud M. Elaasser, Marwa M. Abdel-Aziz (2014): Improvement of antibacterial activity of some sulfa drugs through linkage to certain phthalazin-1(2H)-one scaffolds. European Journal of Medicinal Chemistry 08/2014; 85:480., DOI:10.1016/j.ejmech.2014.08.016
55. M. M. Ghorab, M. S. Alsaid, M. S. A. El-Gaby, N. A. Safwat, M. M. Elaasser, A. M. Soliman, Eur. J. Med. Chem., 2016, 124, 299–310.